

A Theoretical Framework for Iteratively Enhanced Room-Temperature Single-Photon Detection

Hao Shu*
Sun Yat-Sen University

High-performance photon detection is indispensable in a wide range of quantum-optical applications and is conventionally treated as a fixed device-level operation based on single-photon detectors (SPDs). However, state-of-the-art SPDs rely on superconducting materials, which impose severe technological demands and require challenging operational conditions such as cryogenic cooling, thereby hindering scalable implementation. Here, we propose the enhanced single-photon detector (ESPD) framework, a theoretical paradigm supported by numerical simulations, that reformulates single-photon detection as an iteratively enhanced process based on state preparation, controlled operations, projective measurements, and multi-copy analysis, and enables substantial performance improvement using exclusively room-temperature components. Numerical simulations indicate that, within a physically motivated parameter regime, the ESPD framework can upgrade a legacy SPD with a detection efficiency (DE) of about 59% and a dark count rate (DCR) of about 10^{-2} to effective performance metrics with DE exceeding 93% and DCR below 10^{-9} , comparable to those of superconducting SPDs. As a consequence, the minimal tolerable channel transmission rate for quantum key distribution protocols can be reduced by several orders of magnitude. While its physical realization would require substantial experimental integration, the ESPD framework establishes a general system-level perspective on photon detection, highlighting the potential of iterative quantum processing for overcoming intrinsic detector limitations at room temperature.

I. INTRODUCTION

Single-photon detection plays a central role in quantum optics and underlies a wide range of quantum-optical applications. Conventionally, the detection process is treated as a fixed device-level operation implemented by single-photon detectors (SPDs). The two most critical performance metrics of an SPD are the detection efficiency (DE), denoted by η , and the dark count rate (DCR), denoted by d . The former affects the efficiency of nearly all quantum operations, while the latter imposes the ultimate limitation in high-attenuation scenarios. In terms of DE, numerous quantum experiments rely on SPD signals to retrieve results. In linear optical quantum computation, where success events are probabilistic and require the simultaneous detection of multiple photons, the success rate decreases exponentially with low-efficiency SPDs [1–3]. In Bell tests for quantum non-locality, verifying violations of the Clauser–Horne–Shimony–Holt or Eberhard inequalities routinely requires DE exceeding specific thresholds to close loopholes [4–10], such as approximately 67% [11] or 83% [12]. In heralded single-photon sources, where entangled pairs are generated, and one photon is detected to confirm the presence of the other, the efficiency of the SPD directly dictates the success rate [13–16]. With respect to DCR, a primary constraint arises in quantum communication, particularly in quantum key distribution (QKD). The security of a practical QKD protocol relies on maintaining the quantum bit error rate (QBER) below a protocol-specific threshold, significantly lower than 50% [17–20].

However, communication channels induce exponential photon attenuation [21–24]. If the effective signal rate, determined by the channel transmission rate and thus communication distance, falls below the DCR of the SPDs, the QBER rises precipitously, as dark count events (which yield a 50% error rate) dominate the detection statistics. Consequently, the practical secure distance of QKD is strictly limited by the DCR of the SPDs [25–27].

Driven by their critical importance, SPD has remained a continuous research focus since the inception of quantum technologies. While capable of operating at room temperature, traditional SPDs often suffer from both low DE and high DCR. For instance, a frequency upconversion SPD presented in 2004 operates at 300 K with DE about 59% and DCR of 10^{-2} [28], while an InGaAs/InP SPD presented in 2017 operates at 223 K with DE about 27.5% and DCR of 10^{-6} [29]. Such specifications are insufficient for advanced quantum tasks, which typically require the DE of SPD above 90% with DCR below 10^{-7} .

To suppress DCR and enhance DE, recent efforts have shifted toward designing SPDs using superconducting devices, such as superconducting nanowire SPDs (SNSPDs) [30–33]. These SPDs achieve performance superior to traditional counterparts, boosting DE to over 90% while suppressing DCR by several orders of magnitude. This capability enables the implementation of demanding quantum tasks, such as long-distance QKD [19, 34–36]. A summary of recent representative advancements in superconducting SPDs is presented in Table I.

However, as illustrated in the table, the reliance on superconductors necessitates stringent operating conditions, specifically with extremely low temperatures. When these demanding conditions are relaxed, the SPD performance degrades significantly. This require-

* Hao_B_Shu@163.com(Primary),
shuh6@mail.sysu.edu.cn(Alternative)

TABLE I: Summary of recent representative performance benchmarks for state-of-the-art superconducting SPDs. OT: Operation Temperature, DE: Detective efficiency, DCR: Dark count rate.

Year	Researchers (et al.)	OT	DE	DCR
2020	P. Hu [30]	2.10 K	95.0 %	0.5×10^{-5}
2021	J. Chang [31]	2.50 K	99.5 %	1.1×10^{-3}
2021	G. Z. Xu [32]	0.84 K	92.2 %	3.6×10^{-5}
2023	I. Craiciu [33]	0.90 K	78.0 %	1.0×10^{-7}
2024	I. Charaev [37]	20.0 K	7.60 %	1.0×10^{-3}

ment introduces significant infrastructural requirements and operational complexity, fundamentally hindering the scalability and widespread implementation of high-performance quantum technology in field-deployable and environmentally constrained situations.

To address the limitations imposed by the suboptimal performance of room-temperature SPDs and cryogenic operation in superconducting alternatives, we propose the enhanced single-photon detector (ESPD) framework, a system-level theoretical paradigm supported by numerical simulations for improving single-photon detection using exclusively room-temperature components. The ESPD framework reformulates single-photon detection as an iteratively enhanced process rather than a fixed device-level operation, in which detection performance is progressively improved through the integration of state preparation, controlled operations, projective measurements, and multi-copy analysis. As a representative numerical benchmark, we show that, within a physically motivated parameter regime, the ESPD framework can enhance a legacy non-superconducting SPD reported two decades ago [28], upgrading an initial detector with DE of about 59% and DCR of 10^{-2} to effective performance metrics with DE exceeding 93% and DCR below 10^{-9} . These values are comparable to those of state-of-the-art superconducting SPDs and relax the minimal tolerable channel transmission rate for quantum key distribution by several orders of magnitude. While the physical realization of such an architecture would require substantial experimental integration, the ESPD framework provides a general platform for the theoretical and numerical investigation of enhancement mechanisms in room-temperature photon detection, highlighting the way in which system-level quantum processing can overcome intrinsic device limitations.

II. METHOD AND RESULT

In this section, we detail the architecture of the Enhanced Single-Photon Detector (ESPD) scheme, which iteratively improves performance initialized from a base (existing) SPD. We establish the theoretical framework governing its operation, provide analytical approximations to characterize its performance, and state its appli-

cations in QKD.

A. Paradigm of the Enhanced Single-Photon Detection

The ESPD architecture is designed to recursively upgrade the capabilities of a given SPD level by level, ultimately achieving high DE and low DCR.

For clarity, we clarify that DE is the probability of generating a positive detection event given a non-vacuum (single-photon) input, and the DCR is the probability of a positive report given a vacuum input. Let ESPD_s denote the ESPD at level s , with DE η_s and DCR d_s . The iteration begins with an initial existing SPD, ESPD_0 , characterized by initial value $\eta_0 = \eta$ and $d_0 = d$.

With qubit logic, the schematic of the ESPD paradigm is illustrated in Fig. 1.

The construction of the $(s + 1)$ -th level detector, ESPD_{s+1} , proceeds as follows. To facilitate understanding, readers can consider an implementation where the degree of freedom (DOF) is photon polarization and the controlled operations are C-NOT gates.

- DOF Selection:** Select a manipulable DOF of the incoming photon (e.g., polarization). Let $\{|0\rangle, |1\rangle\}$ denote the computational basis for this DOF. We treat the signal as a qutrit in the basis $\{|\emptyset\rangle, |0\rangle, |1\rangle\}$, where $|\emptyset\rangle$ denotes the vacuum state, and $|0\rangle, |1\rangle$ denote the orthonormal states of a non-vacuum photon¹.
- State Preparation:** Apply a state preparation operation to the incoming signal to initialize the selected DOF to $|1\rangle$. Consequently, a non-vacuum signal is mapped to $|1\rangle$, while a vacuum signal remains $|\emptyset\rangle$.
- Controlled Operations:** Implement n_{s+1} controlled operations, denoted as $C(F_i)$ for $i = 1, \dots, n_{s+1}$ (typically C-NOT gates). These gates interact the signal path with n_{s+1} auxiliary sources, each initialized in the state $|0\rangle$.
- Auxiliary Measurement:** Perform projective measurements on the auxiliary outputs in the basis $\{|0\rangle, |1\rangle\}$. Outcome paths of $|0\rangle$ are discarded, and only the $|1\rangle$ paths are preserved for detection.
- Detection:** Detect the signals at the end of paths, including the signal one and the auxiliary ones, using s -th level detectors, ESPD_s .

¹ Note that if the selected DOF is the photon number itself, $|0\rangle$ coincides with $|\emptyset\rangle$ and $|1\rangle$ represents non-vacuum, which degenerates to the qubit case. However, for practical implementations, it is often more convenient to use an internal DOF like polarization distinct from photon existence.

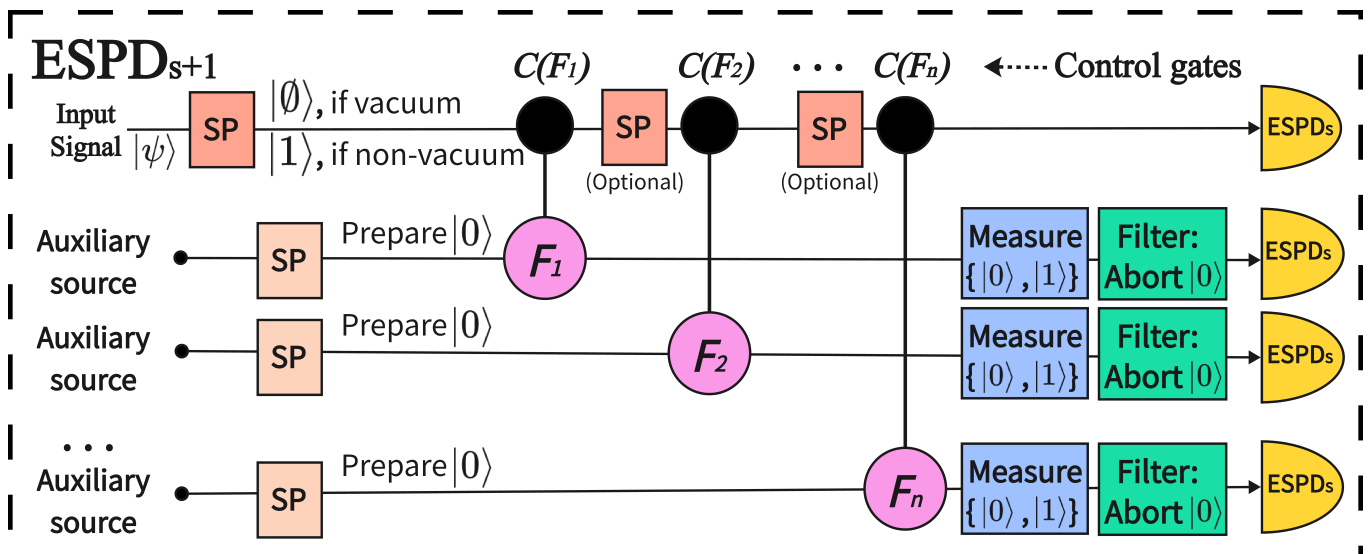


FIG. 1: Schematic representation of the recursive ESPD architecture. The $(s + 1)$ -th level detector (ESPD_{s+1}) is constructed by integrating multiple copies of the s -th level detector (ESPD_s) with controlled gates. Here, $C(F_i)$ are controlled gates, SP are state-preparation operations, measurements are projective measurements via basis $\{|0\rangle, |1\rangle\}$, and filters represent that the $|0\rangle$ path is aborted.

6. **Decision Logic:** A positive detection report for ESPD_{s+1} is generated if and only if at least k_{s+1} positive detections are registered among the $n_{s+1} + 1$ detectors (comprising n_{s+1} auxiliary detectors and one signal path detector). Otherwise, a negative report is returned. Here, k_{s+1} is a pre-selected threshold integer, and n_{s+1} refers to the number of effective operations².

Physical intuition: Intuitively, each level of the ESPD framework increases the number of effective detection opportunities for an input signal, thereby enhancing the overall detection capability. In an idealized limit where all components except the SPDs are assumed to be perfect, the $(s + 1)$ -th level generates n_{s+1} identical copies of the incoming signal by the controlled modules, which are independently detected by n_{s+1} SPDs. A non-vacuum outcome is reported if at least k_{s+1} positive detection events are registered. Under this idealized assumption, the detection efficiency can be enhanced by choosing a small threshold k_{s+1} , for example, when $k_{s+1} = 1$, the effective DE becomes $1 - (1 - \eta_s)^{n_{s+1}}$. Furthermore, the DCR is strongly suppressed, since a false positive outcome occurs only when dark-count events arise in at least k_{s+1} detectors, leading to an approximate scaling $d_s^{k_{s+1}}$, which decreases dramatically when k_{s+1} is

² For example, if the controlled gates are deterministic, then n_{k+1} is exactly the number of used operations, while if the controlled gates are probabilistic, then n_{k+1} refers to the successful ones after post-selection. Therefore, the decision logic is essentially that the positive report rate (among all effective reports) on the multiple detections reaches a pre-defined threshold.

increased. This physical intuition remains valid beyond the idealized limit. When imperfections in the auxiliary components introduce errors that are sufficiently small relative to the activation probability of a genuine input signal, the ESPD framework continues to improve detection performance. A rigorous formulation of this behavior, accounting for non-ideal devices and error propagation, is developed in Section II B.

B. Theoretical Formulations

The rigorous theoretical formulation of the ESPD framework is developed in this subsection. We first introduce the notations and assumptions, and then present the exact analytical expressions.

1. Notations and Basic Assumptions

We define the parameters governing the system dynamics. As stated, η_s and d_s represent the DE and DCR of ESPD_s , respectively. Although η_s may depend on the photon number distribution, we approximate it as a unified value for the given system for simplicity. The parameters n_{s+1} and k_{s+1} denote the number of effective controlled operations and the decision threshold for ESPD_{s+1} , respectively.

For convenience, assume that all controlled operations $C(F_i)$ are identical, denoted simply as $C(F)$, and they are implemented in a feedforward controlled configuration, which ensures that n_{s+1} represents both the number of effective modules and the total physical modules

required for level $s + 1$. However, we emphasize that the generalized ESPD paradigm remains valid for post-selection controlled gates (for a brief discussion, see Section III A 2). Let p be the transmission probability of the signal path through a single module (an (optional) state preparation followed by a $C(F)$). Specifically, p is the probability that the output signal remains non-vacuum given a non-vacuum input of a single non-cascaded module, accounting for loss but irrespective of decoherence (since the state can be re-prepared). Let P and Q denote the probabilities of obtaining a non-vacuum output on the controlled path before detection, given that the input to the corresponding module was non-vacuum or vacuum, respectively. Hence, Q represents the intrinsic error rate of the auxiliary path in the absence of $C(F)$ (i.e., errors from auxiliary state preparation and measurement (SPAM), but not including detection). We approximately assume p , P , and Q are invariant across all $C(F)$ module operations.

It is crucial to note that p , P , and Q represent the intrinsic performance metrics of a single, non-cascaded controlled module. These parameters are defined at the component level and remain invariant with respect to the number of cascaded modules. The cumulative effects of loss and error due to the system's cascaded architecture will be fully incorporated into the derived system equations, such as η_{s+1} in Eq.(6).

2. Parameter Approximation Assumptions

The assumptions below are employed solely to derive analytical approximations in Section II C, as well as the approximation part in Eq. (1) and (2). They are not required for the general theoretical formulation of the ESPD framework nor for the numerical simulations presented in this work. Although these assumptions entail relatively stringent requirements, they are physically motivated by realistic components and will be discussed in detail in Section III A.

In practical scenarios, SPD DE typically ranges from 10% to 90%, while the DCR is generally below 10^{-3} . Consequently, the hierarchy $0 \leq d \ll \eta \leq 1$ holds. We further assume $d_s \ll P\eta_s$, which is trivial: If it were violated, the signal contribution from the controlled operations would become indistinguishable from device noise, rendering the operations practically insignificant. Additionally, we assume that the transmission rate of a single controlled module $p \approx 1$, SPAM error of the auxiliary path $Q \ll 1$, given the maturity of commercial optical components (see Section III A). Finally, considering practical implementation costs, we assume n_s and k_s are moderate integers satisfying $1 \leq k_s \leq n_s$.

3. Formulations

Let P_s and Q_s denote the probabilities of obtaining a positive report on an auxiliary path given a non-vacuum or vacuum input to a $C(F)$ module, respectively, using ESPD_s as the detector. They can be expressed as:

$$\begin{aligned} P_{s+1} &= P[\eta_s + (1 - \eta_s)d_s] + (1 - P)d_s \\ &= P\eta_s(1 - d_s) + d_s \approx P\eta_s \end{aligned} \quad (1)$$

$$\begin{aligned} Q_{s+1} &= Q[\eta_s + (1 - \eta_s)d_s] + (1 - Q)d_s \\ &= Q\eta_s(1 - d_s) + d_s \approx Q\eta_s + d_s \leq Q + d_s \end{aligned} \quad (2)$$

Similarly, let P'_s and Q'_s denote the probabilities of obtaining a positive report on the signal path after all $C(F)$ operations, given a non-vacuum or vacuum output from the final controlled gate, respectively, then:

$$P'_{s+1} = \eta_s + (1 - \eta_s)d_s \approx \eta_s, \quad Q'_{s+1} = d_s \quad (3)$$

We now derive the DE and DCR for the $(s+1)$ -th level.

For the DE calculation, we assume a non-vacuum input and calculate the probability of obtaining at least k_{s+1} positive reports out of $n_{s+1} + 1$ total detections. If the photon is lost exactly after the i -th $C(F)$, the probability of a final positive report is:

$$\begin{aligned} P_{s+1, k_{s+1}, i} &= (1 - Q'_{s+1}) \sum_{j_1 + j_2 = k_{s+1}}^{n_{s+1}} \binom{i}{j_1} P_{s+1}^{j_1} (1 - P_{s+1})^{i-j_1} \binom{n-i}{j_2} Q_{s+1}^{j_2} (1 - Q_{s+1})^{n-i-j_2} \\ &\quad + Q'_{s+1} \sum_{j_1 + j_2 = k_{s+1} - 1}^{n_{s+1}} \binom{i}{j_1} P_{s+1}^{j_1} (1 - P_{s+1})^{i-j_1} \binom{n-i}{j_2} Q_{s+1}^{j_2} (1 - Q_{s+1})^{n-i-j_2} \end{aligned} \quad (4)$$

where the first and second terms correspond to scenarios that the signal path detector reports negative and positive, respectively.

where the first and second terms correspond to scenarios that the signal path detector reports negative and positive, respectively.

If the photon survives all $C(F)$ operations, the probability of a final positive report is:

$$\begin{aligned}
P_{s+1,k_{s+1}} &= P'_{s+1} \sum_{j \geq k_{s+1}-1} \binom{n_{s+1}}{j} P_{s+1}^j (1 - P_{s+1})^{n_{s+1}-j} + (1 - P'_{s+1}) \sum_{j \geq k_{s+1}} \binom{n_{s+1}}{j} P_{s+1}^j (1 - P_{s+1})^{n_{s+1}-j} \\
&= P'_{s+1} \binom{n_{s+1}}{k_{s+1}-1} P_{s+1}^{k-1} (1 - P_{s+1})^{n_{s+1}-k_{s+1}+1} + \sum_{j \geq k_{s+1}} \binom{n_{s+1}}{j} P_{s+1}^j (1 - P_{s+1})^{n_{s+1}-j}
\end{aligned} \tag{5}$$

Combining these, the DE of ESPD_{s+1} is:

$$\eta_{s+1} = p^{n_{s+1}} P_{s+1,k_{s+1}} + \sum_{i=1}^{n_{s+1}} p^{i-1} (1-p) P_{s+1,k_{s+1},i} \tag{6}$$

For the DCR calculation, we assume a vacuum input. The probability of a false positive is:

$$\begin{aligned}
d_{s+1} &= (1 - Q'_{s+1}) \sum_{j \geq k_{s+1}} \binom{n_{s+1}}{j} Q_{s+1}^j (1 - Q_{s+1})^{n_{s+1}-j} \\
&\quad + Q'_{s+1} \sum_{j \geq k_{s+1}-1} \binom{n_{s+1}}{j} Q_{s+1}^j (1 - Q_{s+1})^{n_{s+1}-j}
\end{aligned} \tag{7}$$

Collectively, the DE and DCR evolution is governed by the non-linear time-variant dynamic system:

$$(\eta_{s+1}, d_{s+1}) = G_{s+1}(\eta_s, d_s), \quad (\eta_0, d_0) = (\eta, d) \tag{8}$$

where the map G_{s+1} is defined by Eq. (1) to (7).

$$\begin{aligned}
&\frac{d}{dx} f(x) \\
&= x^{k-2} \left[\binom{n}{k-1} a (1-x)^{n-k} [(k-1)(1-x) - x(n-k+1)] + \sum_{j \geq k} \binom{n}{j} [j x^{j+1-k} (1-x)^{n-j} - x^{j-k+2} (1-x)^{n-j-1} (n-j)] \right] \\
&= x^{k-2} \left[\binom{n}{k-1} a (1-x)^{n-k} (k-1-nx) + \sum_{j \geq k} \binom{n}{j} x^{j+1-k} (1-x)^{n-j-1} (j-nx) \right] \\
&\geq x^{k-2} \left[\binom{n}{k-1} a (1-x)^{n-k} + \sum_{j \geq k} \binom{n}{j} x^{j+1-k} (1-x)^{n-j-1} \right] (k-1-nx) \geq 0
\end{aligned} \tag{11}$$

■

Applying the upper bound from Eq. (2), substituting

C. Analytical Approximations and Stability Analysis

While Eq. (8) describes the exact dynamics, an analytical solution is generally intractable. However, employing the approximations in Eq.(1) to (3) and the assumptions from Section IIB2, we can derive simplified bounds to elucidate the system's behavior.

Consider the DCR evolution. Eq. (7) can be reformulated as:

$$\begin{aligned}
d_{s+1} &= Q'_{s+1} \binom{n_{s+1}}{k_{s+1}-1} Q_{s+1}^{k-1} (1 - Q_{s+1})^{n_{s+1}-k_{s+1}+1} \\
&\quad + \sum_{j \geq k_{s+1}} \binom{n_{s+1}}{j} Q_{s+1}^j (1 - Q_{s+1})^{n_{s+1}-j}
\end{aligned} \tag{9}$$

Proposition 1. Define the function

$$f(x) = a \binom{n}{k-1} x^{k-1} (1-x)^{n-k+1} + \sum_{j \geq k} \binom{n}{j} x^j (1-x)^{n-j} \tag{10}$$

Then $f(x)$ is monotonically increasing for $x \in [0, \frac{k-1}{n}]$.

Proof: For $x \in [0, \frac{k-1}{n}]$:

Eq. (3) to Eq. (9), and assuming $k-1 \geq nx$, we obtain:

$$d_{s+1} \leq d_s \binom{n_{s+1}}{k_{s+1}-1} (Q + d_s)^{k_{s+1}-1} (1 - Q - d_s)^{n_{s+1}-k_{s+1}+1} + \sum_{j \geq k_{s+1}} \binom{n_{s+1}}{j} (Q + d_s)^j (1 - Q - d_s)^{n_{s+1}-j} \tag{12}$$

which is notably independent of η_s . Given $Q_s, d_s \ll 1$

and moderate n_{s+1}, k_{s+1} , we assume $\binom{n_{s+1}}{j} (Q + d_s) \ll 1$.

This yields the approximation:

$$d_{s+1} \lesssim d_s \binom{n_{s+1}}{k_{s+1}-1} (Q + d_s)^{k_{s+1}-1} + \binom{n_{s+1}}{k_{s+1}} (Q + d_s)^{k_{s+1}} = (Q + d_s)^{k_{s+1}-1} \left[d_s \binom{n_{s+1}}{k_{s+1}-1} + \binom{n_{s+1}}{k_{s+1}} (Q + d_s) \right] \quad (13)$$

This provides an estimation for the DCR at level $s + 1$.

Similarly, the DE can be lower-bounded by:

$$\begin{aligned} \eta_{s+1} &\geq p^{n_{s+1}} \left[P'_{s+1} \sum_{j \geq k_{s+1}-1} \binom{n_{s+1}}{j} P_{s+1}^j (1 - P_{s+1})^{n_{s+1}-j} + (1 - P'_{s+1}) \sum_{j \geq k_{s+1}} \binom{n_{s+1}}{j} P_{s+1}^j (1 - P_{s+1})^{n_{s+1}-j} \right] \\ &= p^{n_{s+1}} \left[P'_{s+1} \binom{n_{s+1}}{k_{s+1}-1} P_{s+1}^{k_{s+1}-1} (1 - P_{s+1})^{n_{s+1}-k_{s+1}+1} + \sum_{j \geq k_{s+1}} \binom{n_{s+1}}{j} P_{s+1}^j (1 - P_{s+1})^{n_{s+1}-j} \right] \\ &\approx p^{n_{s+1}} \left[\eta_s \binom{n_{s+1}}{k_{s+1}-1} (P\eta_s)^{k_{s+1}-1} (1 - P\eta_s)^{n_{s+1}-k_{s+1}+1} + \sum_{j \geq k_{s+1}} \binom{n_{s+1}}{j} (P\eta_s)^j (1 - P\eta_s)^{n_{s+1}-j} \right] \end{aligned} \quad (14)$$

which is independent of d_s . Therefore, solving the in-

equality

$$p^n (Px)^{k-1} \left[x \binom{n}{k-1} (1 - Px)^{n-k+1} + \sum_{j \geq k} \binom{n}{j} (Px)^{j-k+1} (1 - Px)^{n-j} \right] - x > 0 \quad (15)$$

determines the condition under which the DE is enhanced in the subsequent level. If n_s and k_s are constant across levels and the system is stable, the DE of ESPD $_s$ will converge to a root of the left-hand side of Eq. (15).

D. Performance Simulations

While obtaining an exact analytical solution for the non-linear, time-variant dynamic system governing the ESPD in Eq.(8) is mathematically complex, numerical methods provide a robust and sufficient approach for practical design. In this section, we present numerical simulations for the ESPD paradigm, indicating that substantial performance gains are achievable even with moderate initial hardware specifications. For example, a three-level ESPD can transform a semiconductor SPD into one exhibiting DE $> 93\%$ and DCR $< 10^{-9}$, effectively removing the necessity for superconducting materials while matching or exceeding the performance of state-of-the-art SNSPDs.

Simulation Parameters: We evaluated the performance of the ESPD scheme using two distinct baseline SPDs. The first represents an older technology, characterized by low performance parameters (η_0, d_0) =

(59%, 10^{-2}) [28], while the second represents more modern InGaAs/InP SPD performance, with (η_0, d_0) = (27.5%, 10^{-6}) [29]. Additionally, the controlled-gate parameters are set to $p = 0.98$, which can be achieved by commercial devices [38], and $P = 0.97$, achievable recently by feedforward C-NOT gate implementations in photonic platforms [39–42], while, for the auxiliary path, the error rate is set to $Q = 0.2\%$, justified by the extremely low SPAM errors (without detections) achievable across specific DOF and the inherent design freedom in selecting the appropriate DOF for the ESPD implementation [38, 43] (see Section III A for parameter discussions). We also implemented additional simulations using degraded parameter settings to evaluate robustness (also see Section III A).

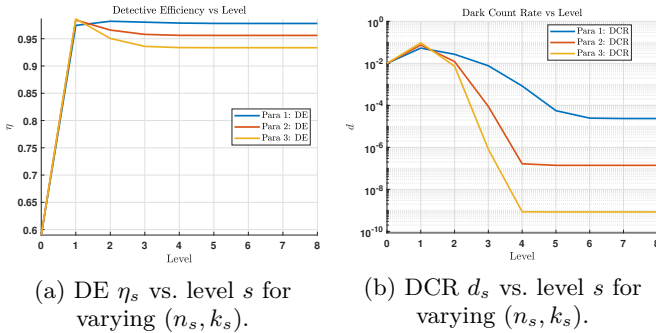
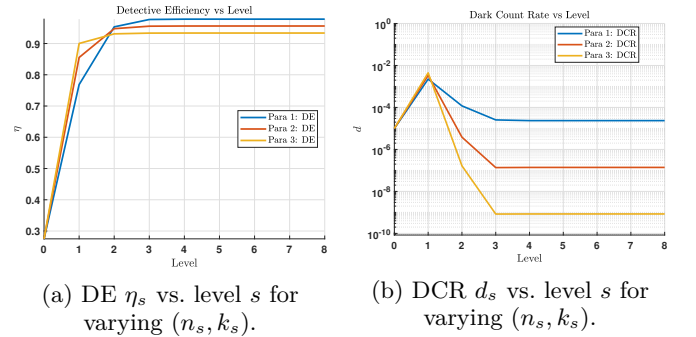
Performance Outcomes: Numerical performance metrics across varying configurations and baseline architectures are summarized in Table II and III with visual representations in Fig. 2 and 3. The results indicate that the ESPD scheme can significantly enhance the capabilities of conventional SPDs. Notably, with only three or four levels of enhancement, the detectors achieve performance metrics (DE $> 93\%$, DCR $< 10^{-9}$) that are comparable to those of advanced superconducting SPDs.

TABLE II: Performance of an ESPD initialized with a SPD from [28], with $\eta_0 = 59\%$, $d_0 = 10^{-2}$.

Level	Para 1		Para 2		Para 3	
	(n, k)	(DE (η), DCR (d))	(n, k)	(DE (η), DCR (d))	(n, k)	(DE (η), DCR (d))
0	-	(59.0%, 1.0×10^{-2})	-	(59.0%, 1.0×10^{-2})	-	(59.0%, 1.0×10^{-2})
1	(4,1)	(97.4%, 5.3×10^{-2})	(6,1)	(98.4%, 7.5×10^{-2})	(8,1)	(98.6%, 9.5×10^{-2})
2	(4,2)	(98.2%, 2.7×10^{-2})	(6,3)	(96.6%, 1.2×10^{-2})	(8,4)	(95.1%, 7.4×10^{-3})
3	(4,2)	(98.0%, 7.7×10^{-3})	(6,3)	(95.8%, 8.9×10^{-5})	(8,4)	(93.6%, 8.1×10^{-7})
4	(4,2)	(97.9%, 8.4×10^{-4})	(6,3)	(95.6%, 1.7×10^{-7})	(8,4)	(93.4%, 8.6×10^{-10})
5	(4,2)	(97.8%, 5.6×10^{-5})	(6,3)	(95.6%, 1.4×10^{-7})	(8,4)	(93.4%, 8.5×10^{-10})
6	(4,2)	(97.8%, 2.5×10^{-5})	(6,3)	(95.6%, 1.4×10^{-7})	(8,4)	(93.4%, 8.5×10^{-10})
7	(4,2)	(97.8%, 2.4×10^{-5})	(6,3)	(95.6%, 1.4×10^{-7})	(8,4)	(93.4%, 8.5×10^{-10})
8	(4,2)	(97.8%, 2.4×10^{-5})	(6,3)	(95.6%, 1.4×10^{-7})	(8,4)	(93.4%, 8.5×10^{-10})

TABLE III: Performance of an ESPD initialized with a SPD from [29], with $\eta_0 = 27.5\%$, $d_0 = 10^{-6}$.

Level	Para 1		Para 2		Para 3	
	(n, k)	(DE (η), DCR (d))	(n, k)	(DE (η), DCR (d))	(n, k)	(DE (η), DCR (d))
0	-	(27.5%, 1.0×10^{-6})	-	(27.5%, 1.0×10^{-6})	-	(27.5%, 1.0×10^{-6})
1	(4,1)	(76.9%, 2.2×10^{-3})	(6,1)	(85.5%, 3.4×10^{-3})	(8,1)	(90.0%, 4.5×10^{-3})
2	(4,2)	(95.3%, 1.2×10^{-4})	(6,2)	(94.8%, 3.8×10^{-4})	(8,4)	(93.1%, 1.7×10^{-7})
3	(4,2)	(97.7%, 2.6×10^{-5})	(6,3)	(95.5%, 1.4×10^{-7})	(8,4)	(93.3%, 8.4×10^{-10})
4	(4,2)	(97.8%, 2.4×10^{-5})	(6,3)	(95.6%, 1.4×10^{-7})	(8,4)	(93.4%, 8.4×10^{-10})
5	(4,2)	(97.8%, 2.4×10^{-5})	(6,3)	(95.6%, 1.4×10^{-7})	(8,4)	(93.4%, 8.5×10^{-10})
6	(4,2)	(97.8%, 2.4×10^{-5})	(6,3)	(95.6%, 1.4×10^{-7})	(8,4)	(93.4%, 8.5×10^{-10})
7	(4,2)	(97.8%, 2.4×10^{-5})	(6,3)	(95.6%, 1.4×10^{-7})	(8,4)	(93.4%, 8.5×10^{-10})
8	(4,2)	(97.8%, 2.4×10^{-5})	(6,3)	(95.6%, 1.4×10^{-7})	(8,4)	(93.4%, 8.5×10^{-10})

FIG. 2: Performance for initial parameters $\eta_0 = 59.0\%$ and $d_0 = 1.0 \times 10^{-2}$.FIG. 3: Performance for initial parameters $\eta_0 = 27.5\%$ and $d_0 = 1.0 \times 10^{-6}$.

E. Application on QKD

To illustrate the practical impact of the ESPD scheme, we consider its application in QKD. For a QKD protocol having a secure threshold e_{th} and total error rate e_C not accounting for SPDs, the minimal tolerable channel transmission rate γ is conventionally approximated by:

$$\gamma = \frac{(1 - 2e_{th})d}{\eta[e_{th} - e_C + d(1 - 2e)]} \approx \frac{1 - 2e_{th}}{e_{th} - e_C} \frac{d}{\eta} \quad (16)$$

Given that the ESPD paradigm reduces the DCR (d) by several orders of magnitude (even compared to SNSPDs),

it proportionately lowers the minimal tolerable channel transmission rate γ by the same factor. Furthermore, the simultaneous enhancement of the DE (η) not only lowers γ but also translates directly into an improved QKD key rate at any fixed distance.

Compared to the empty-signal-detection paradigm [27], which also reduces the threshold of the minimal tolerable channel transmission rate, the ESPD scheme avoids introducing an extra sifting term that penalizes efficiency. This allows significant QKD performance improvements without additional efficiency costs. Consequently, the ESPD paradigm offers a compelling first-

TABLE IV: Performance of an ESPD initialized with a SPD from [28], with p varied from 0.80 to 0.96. Experiments are run for $(n, k) = (5, 2)$ on each level, and all other settings remain consistent with those described in Section IID.

	$p=0.80$	$p=0.84$	$p=0.88$	$p=0.92$	$p=0.96$
Level	(DE (η), DCR (d))	(DE (η), DCR (d))	(DE (η), DCR (d))	(DE (η), DCR (d))	(DE (η), DCR (d))
0	(59.0%, 1.0×10^{-2})				
1	(60.8%, 1.8×10^{-3})	(66.7%, 1.8×10^{-3})	(72.9%, 1.8×10^{-3})	(79.7%, 1.8×10^{-3})	(87.0%, 1.8×10^{-3})
2	(61.0%, 1.1×10^{-4})	(70.6%, 1.2×10^{-4})	(79.7%, 1.3×10^{-4})	(87.8%, 1.4×10^{-4})	(94.6%, 1.5×10^{-4})
3	(61.0%, 1.8×10^{-5})	(72.6%, 2.4×10^{-5})	(82.1%, 3.1×10^{-5})	(89.5%, 3.7×10^{-5})	(95.4%, 4.3×10^{-5})
4	(60.9%, 1.5×10^{-5})	(73.5%, 2.2×10^{-5})	(82.8%, 2.8×10^{-5})	(89.9%, 3.4×10^{-5})	(95.4%, 3.8×10^{-5})
5	(60.8%, 1.5×10^{-5})	(74.0%, 2.2×10^{-5})	(83.1%, 2.9×10^{-5})	(89.9%, 3.4×10^{-5})	(95.4%, 3.8×10^{-5})
6	(60.8%, 1.5×10^{-5})	(74.2%, 2.3×10^{-5})	(83.2%, 2.9×10^{-5})	(89.9%, 3.4×10^{-5})	(95.4%, 3.8×10^{-5})
7	(60.8%, 1.5×10^{-5})	(74.3%, 2.3×10^{-5})	(83.2%, 2.9×10^{-5})	(89.9%, 3.4×10^{-5})	(95.4%, 3.8×10^{-5})
8	(60.8%, 1.5×10^{-5})	(74.3%, 2.3×10^{-5})	(83.2%, 2.9×10^{-5})	(89.9%, 3.4×10^{-5})	(95.4%, 3.8×10^{-5})

choice solution for practical quantum communication implementations.

III. DISCUSSION

In the absence of experimental implementation, we focus on the technological feasibility and practical robustness of the ESPD framework, and discuss its limitations and directions for future work.

A. Technological Feasibility and Performance under Degraded Parameters

The most significant advantage of the ESPD paradigm lies in its reliance on accessible, room-temperature components, effectively bypassing the cryogenic requirements of superconducting SPDs. The device requirements are discussed as follows.

1. State Preparations and Measurements

The flexibility of the architecture, which allows for various DOF to be employed, enables the selection of an easily manipulated one. In practical implementations, this facilitates state preparation and projective measurement, ensuring that the error parameter Q can be executed with extremely low rates. Specifically, Q can be suppressed to 10^{-4} level using standard optical setups and commercial platforms [38, 43], thereby guaranteeing $Q \ll 1$.

2. Controlled Gates

The primary technological prerequisites of the ESPD scheme are the controlled quantum gates, typically C-NOT operations, which define the critical parameters p and P .

A high transmission efficiency, with attenuation as low as 0.1 dB (corresponding to a propagation probability

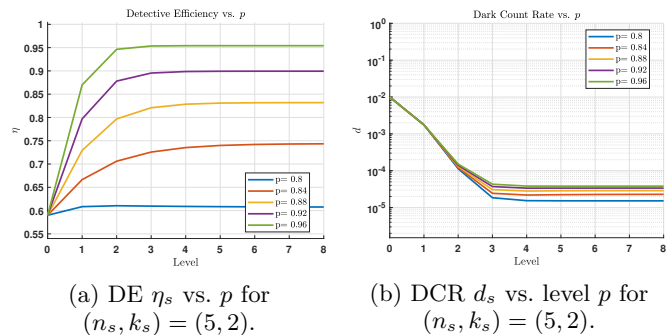


FIG. 4: Performance for parameters $\eta_0 = 59.0\%$, $d_0 = 1.0 \times 10^{-2}$. All other settings remain consistent with those described in Section IID.

$p \approx 0.98$) [38], is achievable with commercial photonic integrated circuits [44–47], suggesting that p can approach unity. It is important to reiterate that p represents the intrinsic transmission rate of a single, non-cascaded controlled module, and consequently, does not decrease with an increasing number of cascaded modules or cascaded levels. The cumulative system loss is fully accounted for in the derivation of the total system efficiency, η_{s+1} (Eq.(6)).

However, to accommodate practical implementations, one may consider using post-selection controlled gates instead of the feedforward configurations. While the ESPD paradigm remains valid for such probabilistic operations, the overall system efficiency is necessarily degraded. Specifically, if the post-selection efficiency of the controlled gate is N , the average transmission rate from one effective module to the next will be $p^{\frac{1}{N}}$. Although a full theoretical calculation for the post-selection case is structurally similar to that established in Section IIB and is not repeated here, the resulting degradation underscores the importance of characterizing system performance under reduced transmission rate. Table IV and Fig.4 indicate that the ESPD framework maintains performance enhancement even when p drops to 0.80 (approximately 1 dB attenuation, corresponding to the loss

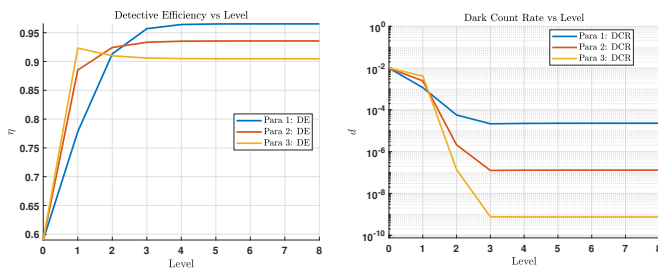
TABLE V: Performance evolution of an ESPD initialized with a baseline detector from [28], with $\eta_0 = 59\%$, $d_0 = 10^{-2}$, and moderate controlled gate fidelity, $P = 0.80$.

Level	Para 1		Para 2		Para 3	
	(n, k)	(DE (η), DCR (d))	(n, k)	(DE (η), DCR (d))	(n, k)	(DE (η), DCR (d))
0	-	(59.0%, 1.0×10^{-2})	-	(59.0%, 1.0×10^{-2})	-	(59.0%, 1.0×10^{-2})
1	(4,2)	(77.8%, 1.2×10^{-3})	(6,2)	(88.5%, 2.4×10^{-3})	(8,2)	(92.3%, 4.2×10^{-3})
2	(4,2)	(91.3%, 5.7×10^{-5})	(6,3)	(92.4%, 2.1×10^{-6})	(8,4)	(91.0%, 1.4×10^{-7})
3	(4,2)	(95.7%, 2.2×10^{-5})	(6,3)	(93.3%, 1.3×10^{-7})	(8,4)	(90.6%, 7.6×10^{-10})
4	(4,2)	(96.4%, 2.3×10^{-5})	(6,3)	(93.5%, 1.3×10^{-7})	(8,4)	(90.5%, 7.5×10^{-10})
5	(4,2)	(96.5%, 5.5×10^{-5})	(6,3)	(93.6%, 1.3×10^{-7})	(8,4)	(90.5%, 7.5×10^{-10})
6	(4,2)	(96.5%, 2.4×10^{-5})	(6,3)	(93.6%, 1.3×10^{-7})	(8,4)	(90.5%, 7.5×10^{-10})
7	(4,2)	(96.5%, 2.3×10^{-5})	(6,3)	(93.6%, 1.3×10^{-7})	(8,4)	(90.5%, 7.5×10^{-10})
8	(4,2)	(96.5%, 2.3×10^{-5})	(6,3)	(93.6%, 1.3×10^{-7})	(8,4)	(90.5%, 7.5×10^{-10})

TABLE VI: Performance evolution of an ESPD initialized with a baseline detector from [28], with $\eta_0 = 59\%$, $d_0 = 10^{-2}$, under a low controlled gate fidelity, $P = 0.40$.

Level	Para 1		Para 2		Para 3	
	(n, k)	(DE (η), DCR (d))	(n, k)	(DE (η), DCR (d))	(n, k)	(DE (η), DCR (d))
0	-	(59.0%, 1.0×10^{-2})	-	(59.0%, 1.0×10^{-2})	-	(59.0%, 1.0×10^{-2})
1	(2,1)	(75.1%, 3.2×10^{-2})	(7,2)	(66.8%, 3.3×10^{-3})	(8,2)	(71.1%, 4.2×10^{-3})
2	(6,2)	(78.2%, 2.1×10^{-2})	(7,2)	(72.8%, 5.4×10^{-4})	(8,2)	(79.6%, 1.0×10^{-3})
3	(6,2)	(79.1%, 9.5×10^{-3})	(7,2)	(77.2%, 9.0×10^{-4})	(8,2)	(84.3%, 2.1×10^{-4})
4	(6,2)	(78.7%, 2.4×10^{-3})	(7,2)	(80.1%, 5.7×10^{-5})	(8,2)	(86.4%, 1.0×10^{-4})
5	(6,2)	(77.7%, 2.9×10^{-5})	(7,2)	(82.0%, 5.8×10^{-5})	(8,2)	(87.2%, 9.5×10^{-5})
6	(6,2)	(76.7%, 5.4×10^{-5})	(7,2)	(83.0%, 6.1×10^{-5})	(8,2)	(87.5%, 9.5×10^{-5})
7	(6,2)	(76.0%, 3.8×10^{-5})	(7,2)	(83.6%, 6.3×10^{-5})	(8,2)	(87.6%, 9.6×10^{-5})
8	(6,2)	(75.4%, 3.7×10^{-5})	(7,2)	(83.9%, 6.4×10^{-5})	(8,2)	(87.7%, 9.6×10^{-5})

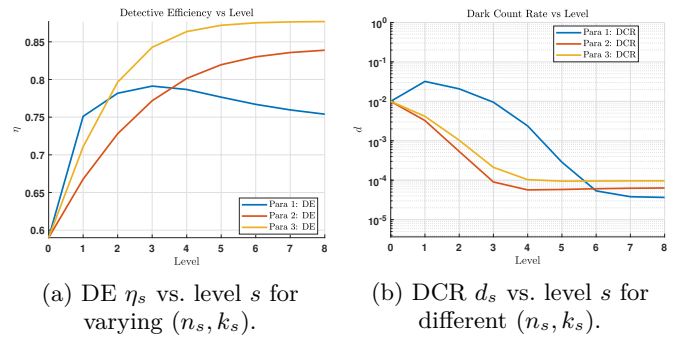
cascaded about 10 controlled modules with 0.1 dB attenuation on each.) This result shows robustness, indicating the scheme's feasibility even for C-NOT gates with a low post-selection efficiency of around 10%, which is well within the reach of current photonic technology [38, 48–52].



(a) DE η_s vs. level s for varying (n_s, k_s) . (b) DCR d_s vs. level s for varying (n_s, k_s) .

FIG. 5: Performance for parameters $\eta_0 = 59.0\%$, $d_0 = 1.0 \times 10^{-2}$, with $P = 0.80$.

We now turn our attention to the parameter P , which is intrinsically linked to the fidelity of the C-NOT gate. Notably, P is lower-bounded by the gate's overall fidelity, as P quantifies deviation only on the controlled path, whereas the full C-NOT fidelity accounts for the cor-



(a) DE η_s vs. level s for varying (n_s, k_s) . (b) DCR d_s vs. level s for varying (n_s, k_s) .

FIG. 6: Performance for parameters $\eta_0 = 59.0\%$, $d_0 = 1.0 \times 10^{-2}$, with $P = 0.40$.

rect operation rate of both the control and controlled paths. Contemporary C-NOT gates demonstrate high fidelities without low-temperature requirement, suggesting that high values of P are readily attainable [38, 48–52]. Specifically, the recent feedforward photonic C-NOT experiment can achieve fidelity over 97% [39–42]. However, it is also worth testing the effectiveness of the paradigm under degraded parameters to indicate its suitability for standard fabrication processes with lower technology requirements. Here, we also provide numerical results for two degraded scenarios: $P = 0.80$ (see Table V with

visual representation in Fig.5, and $P = 0.40$, (see Table VI with visual representation in Fig.6). All other settings remain consistent with those described in Section IID. The numerical results indicate the robustness of the scheme: Comparison of Table V to Table II supports that the ESPD paradigm does not rely on an excessively demanding value for P , since similar substantial performance gains are shown for both $P = 0.97$ and $P = 0.80$, while Table VI implies that the scheme is effective even when the C-NOT fidelity parameter is severely degraded to $P = 0.40$. This robustness indicates that the technological demands of the ESPD method are fully compatible with existing non-superconducting quantum technologies.

3. Choice of initialized SPDs

It is also important to note that the requirements for SPD used for initialization are minimal, further lowering the barrier to implementation. As supported in comparing Table II and III, the stable performance of the ESPD is largely independent of the specific characteristics of the starting detector, provided it falls within a certain convergence interval. The dynamic system described by Eq.(8) exhibits convergence to a stable operational point within this interval, irrespective of the initial point. Moreover, while a trade-off exists between DE and DCR, the DCR of the ESPD can be drastically reduced by increasing k , and the DE can be significantly enhanced by selecting a small k . Therefore, one or two levels of the ESPD paradigm, using suitable n and k , can readily adjust the detector's performance to a desirable operational window, provided the initial SPD is not severely deficient. Indeed, simulations suggest that both an SPD with low DE and low DCR and one with moderate DE and high DCR serve as viable initialization.

In summary, the ESPD scheme only requires a normal, room-temperature SPD for initialization, which is routinely achievable. For instance, even an SPD developed two decades ago [28] is sufficient.

4. Auxiliary Sources

Although nearly perfect sources can be obtained at room temperature [53], indicating that auxiliary sources will not be a barrier, we note that implementing the ESPD scheme may not require single photon sources. The key parameter P represents the detection probability of the state $|1\rangle$ from the auxiliary path with an ideal SPD when the control signal input is non-vacuum, regardless of the exact number of photons or the presence of unwanted $|0\rangle$. Intuitively, multi-photon sources might even offer practical benefits over single-photon sources by providing more opportunities for detecting the required

$|1\rangle$ ³. However, the formulation of this, including its impact on controlled operations, needs a rigorous discussion and is reserved for future work.

B. Limitations and Future Works

Despite the significance of the ESPD framework, some limitations remain and warrant future investigation.

1. Theoretical Completeness

The theoretical framework established in Section IIB remains an area for deeper exploration. While the numerical designs presented in Section IID are sufficient for guiding physical implementation, a complete theoretical study of the dynamic system in Eq.(8) remains of fundamental academic interest. Future work should focus on rigorously deducing the exact convergence conditions, calculating the precise steady-state point, and identifying the minimum initial performance criteria required. Given the inherent mathematical difficulty of such a non-linear and time-variant system and the sufficiency for practical technology employments by numerical designs, these specialized mathematical studies are reserved for the future.

2. Resource Overhead vs. Environmental Simplicity

While the parallelized nature of the ESPD's detection stages theoretically preserves efficiency, the recursive architecture introduces a resource overhead that scales with the number of levels. Specifically, an L -level ESPD utilizing n auxiliary signals per level requires a total of $(n+1)^L$ base detections. Although effective performance is typically achievable with moderate depth ($L = 2$ or 3), this inherent scaling significantly expands the physical footprint and component count compared to a single SNSPD. For instance, a three-level ESPD scheme employing five controlled gates per level ($n = 5$) necessitates $6^3 = 216$ detections (if not applying techniques such as multiplexing), resulting in hundreds of integrated components. While not posing a fundamental physical barrier (as discussed in Section III A), this resource-intensive nature introduces a non-trivial engineering challenge for immediate large-scale deployment.

³ Since the employment of the filter block, for a non-vacuum input of a controlled module, if the auxiliary multi-photon signal results in more state $|1\rangle$, then a positive report has a higher chance to be produced, which provides benefits since it enlarges P , while, if the auxiliary multi-photon signal adds state $|0\rangle$, then they will be filtered out, thus providing no effects. Similarly, for a vacuum input of a controlled module, only $|0\rangle$ is added in auxiliary sources, which will be filtered out and thereby have no effect even if the source is multiple-photon.

TABLE VII: Performance evolution of an ESPD initialized with a baseline detector from [28], with $\eta_0 = 59\%$, $d_0 = 10^{-2}$, under varied (n, k) . Settings are the same as those in Section IID

Level	Para 4		Para 5		Para 6	
	(n, k)	(DE (η), DCR (d))	(n, k)	(DE (η), DCR (d))	(n, k)	(DE (η), DCR (d))
0	-	(59.0%, 1.0×10^{-2})	-	(59.0%, 1.0×10^{-2})	-	(59.0%, 1.0×10^{-2})
1	(8,2)	(95.0%, 4.2×10^{-3})	(4,2)	(86.1%, 1.2×10^{-3})	(3,1)	(95.8%, 4.3×10^{-2})
2	(8,4)	(93.5%, 1.4×10^{-7})	(8,4)	(92.6%, 6.4×10^{-9})	(6,4)	(93.9%, 1.2×10^{-4})
3	(8,4)	(93.4%, 8.5×10^{-10})	(8,4)	(93.3%, 8.2×10^{-10})	(8,4)	(93.4%, 1.2×10^{-9})
4	(8,4)	(93.4%, 8.5×10^{-10})	(8,4)	(93.3%, 8.4×10^{-10})	(8,4)	(93.4%, 8.5×10^{-10})
5	(8,4)	(93.4%, 8.5×10^{-10})	(8,4)	(93.4%, 8.5×10^{-10})	(8,4)	(93.4%, 8.5×10^{-10})
6	(8,4)	(93.4%, 8.5×10^{-10})	(8,4)	(93.4%, 8.5×10^{-10})	(8,4)	(93.4%, 8.5×10^{-10})
7	(8,4)	(93.4%, 8.5×10^{-10})	(8,4)	(93.4%, 8.5×10^{-10})	(8,4)	(93.4%, 8.5×10^{-10})
8	(8,4)	(93.4%, 8.5×10^{-10})	(8,4)	(93.4%, 8.5×10^{-10})	(8,4)	(93.4%, 8.5×10^{-10})

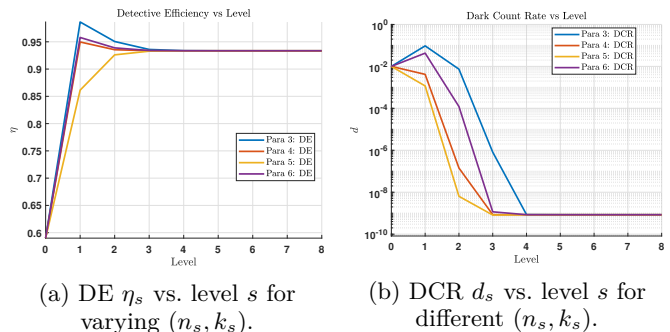
However, this complexity is well within the capabilities of modern large-scale photonic integrated circuits. Recent advances have successfully demonstrated the integration of hundreds to thousands of components on single chips [54–57]. Notably, very-large-scale integration of quantum photonics has been experimentally realized with over 2,500 components on a single silicon-on-insulator chip [58], verifying that the component density required for a multi-level ESPD is manufacturable using standard complementary metal-oxide-semiconductor processes. Furthermore, concerns regarding cumulative loss in cascaded logic gates can be mitigated by emerging low-loss material platforms. For instance, silicon nitride waveguides have demonstrated propagation losses as low as 0.2 dB/cm in complex programmable processors [59], and thin-film lithium niobate platforms offer ultra-low losses of approximately 0.06 dB/cm alongside high-speed modulation capabilities [60].

In summary, the hardware complexity of the ESPD should be evaluated as a deliberate engineering trade-off against the necessity of cryogenic operation. The SNSPD paradigm mandates bulky, energy-intensive, and expensive cryogenic infrastructure (typically operating below 4 K). The ESPD scheme, conversely, shifts the burden from a demanding operating environment to the domain of on-chip integration. By leveraging large-scale photonic platforms, thousands of components can be lithographically fabricated on a single chip, effectively converting high operational costs and environmental constraints into a one-time design and fabrication cost. This trade-off is particularly advantageous for applications where size, weight, and power constraints prohibit the use of cryogenics, such as satellite-based quantum communication payloads, mobile quantum nodes, or research laboratories lacking dedicated low-temperature facilities.

3. Optimization Design

The inherent exponential resource scaling discussed in Section IIIB2 necessitates optimization for future practical deployments. Specifically, the design of the ESPD

requires balancing performance metrics (DE, DCR) against implementation complexity (L, n, k). Reducing the number of levels (L) by even one step can result in significant savings in component count and system complexity due to the $(n+1)^L$ dependence. As shown in Section IID, the optimal choice of parameters n (number of auxiliary signals in each level) and k (decision threshold) is crucial: enlarging k reduces DCR exponentially, while improving DE requires a lower k and a larger n , with the trade-off being that enlarging n increases detection cost. Furthermore, as shown in Table VII and visualized in Fig.7, with a suitably selected n, k on each level, the convergence speed can be accelerated, and the middle-level performance can be adjusted, which is crucial for saving costs.



(a) DE η_s vs. level s for varying (n_s, k_s) . (b) DCR d_s vs. level s for different (n_s, k_s) .

FIG. 7: Performance for parameters $\eta_0 = 59.0\%$, $d_0 = 1.0 \times 10^{-2}$, with different k . Para 3 is the same as in Fig.2.

The optimization problem also encompasses the optimal circuit topology. To mitigate cumulative error propagation, minimizing the maximal circuit length is essential. As the controlled modules' order can be changed and the auxiliary signals behave similarly to the control signal⁴, alternative designs could involve leveraging

⁴ This justifies the dedicated filter block within the paradigm: For

a binary-tree structure and defining the positive report event via a global decision criterion, rather than the current level-by-level n -length structure with local (level-wise) criterion used in Section II A. However, these architectural changes introduce new theoretical challenges: the general binary-tree structure may result in non-independent distributions that are difficult to analyze, and the global decision criterion selection must carefully account for both device requirements and implementation convenience.

4. *Physical Integrations and Experiments*

Despite the convincing indication of effectiveness via numerical simulations in Section II D, physical implementations of the ESPD scheme require dedicated experimental validations. Reassuringly, as established in Section III A, the scheme relies only on readily available conventional quantum optical components, suggesting no fundamental technological barriers are preventing its realization. However, the realization of the large-scale iterative circuit demands significant and focused engineering efforts, particularly concerning the precise integration and synchronization of the cascaded components. Furthermore, the seamless integration of the enhanced detector into various quantum optical tasks (such as QKD) needs full investigation. Thus, both the physical realization of the ESPD scheme and the characterization of its performance in applied scenarios are key directions for future work.

5. *Count Rate and Timing Jitter*

While the ESPD framework significantly enhances DE and suppresses DCR, it generally inherits the timing characteristics of the baseline detectors. Specifically, the system's timing jitter and maximum count rate remain constrained by the intrinsic performance of the initial SPDs (e.g., the avalanche buildup time and dead time of InGaAs/InP devices). However, the architecture does not impose significant additional penalties: the optical-controlled quantum operations function on timescales usually faster than the electronic response of room-temperature SPDs, ensuring negligible added temporal broadening. Furthermore, as the final SPDs operate in parallel, the effective system throughput remains comparable to that of the constituent devices. Nevertheless, future iterations of the ESPD scheme could incorporate techniques such as multiplexing strategies to optimize these temporal metrics.

the controlled gate be C-NOT, the auxiliary output state is $|1\rangle$ if the input signal is non-vacuum, while is $|\emptyset\rangle$ if the input signal is vacuum, theoretically consistent to the input signal after state-preparation.

IV. CONCLUSION

We have introduced the enhanced single-photon detector (ESPD) framework, which reformulates single-photon detection as an iteratively enhanced process based on integrating state preparations, controlled operations, projective measurements, and multi-copy analysis, rather than as a fixed device-level operation. Within this system-level theoretical framework, detector performance is progressively improved through structured quantum processing using exclusively non-superconducting, room-temperature components. Numerical simulations indicate that, starting from a conventional non-superconducting SPD, the ESPD framework can substantially enhance DE while strongly suppressing DCR, yielding effective performance metrics comparable to those of state-of-the-art superconducting SPDs, and significantly relaxing the minimal tolerable channel transmission rate in quantum communication. The ESPD framework makes explicit the trade-off between resource overhead and operating conditions, replacing cryogenic infrastructure with circuit integration complexity. While the experimental realization of large-scale ESPD architectures will require substantial engineering effort, the parameter studies presented in this work, grounded in the performance of existing photonic components, support the in-principle viability of the framework. In essence, this work establishes a system-level perspective on photon detection, showing that intrinsic device limitations can be transcended through iterative quantum processing and providing a principled foundation for the development of high-performance, room-temperature SPDs.

DATA AND CODE AVAILABILITY

All data/codes generated or used during this study are included in this published article or can be found at <https://github.com/Hao-B-Shu/ESPD>.

AUTHOR CONTRIBUTIONS

Hao Shu (the unique author): study design, investigation, experiment, analysis, manuscript preparation.

DECLARATIONS

The author declares no competing interests.

- [1] E. Knill, R. Laflamme, and G. A. Milburn, scheme for efficient quantum computation with linear optics, *Nature* **409**, 46–52 (2001).
- [2] X. Ding, Y. P. Guo, M. C. Xu, R. Z. Liu, G. Y. Zou, J. Y. Zhao, Z. X. Ge, Q. H. Zhang, H. L. Liu, L. J. Wang, M. C. Chen, H. Wang, Y. M. He, Y. H. Huo, C. Y. Lu, and J. W. Pan, High-efficiency single-photon source above the loss-tolerant threshold for efficient linear optical quantum computing, *Nature Photonics* **19**, 387–391 (2025).
- [3] M. Silva, M. Rötteler, and C. Zalka, Thresholds for linear optics quantum computing with photon loss at the detectors, *Physical Review A* **72**, 032307 (2005).
- [4] N. Gisin and B. Gisin, A local hidden variable model of quantum correlation exploiting the detection loophole, *Physics Letters A* **260**, 323 (1999).
- [5] I. Márton, E. Bene, and T. Vértesi, Bounding the detection efficiency threshold in bell tests using multiple copies of the maximally entangled two-qubit state carried by a single pair of particles, *Physical Review A* **107**, 022205 (2023).
- [6] M. T. Quintino, M. Araújo, D. Cavalcanti, M. F. Santos, and M. T. Cunha, Maximal violations and efficiency requirements for bell tests with photodetection and homodyne measurements, *Journal of Physics A: Mathematical and Theoretical* **45**, 10.1088/1751-8113/45/21/215308 (2012).
- [7] T. Vértesi, S. Pironio, and N. Brunner, Closing the detection loophole in bell experiments using qudits, *Physical Review Letters* **104**, 060401 (2010).
- [8] M. A. Rowe, D. Kielpinski, V. Meyer, C. A. Sackett, W. M. Itano, C. Monroe, and D. J. Wineland, Experimental violation of a bell’s inequality with efficient detection, *Nature* **409**, 791–794 (2001).
- [9] W. C. Ma, Efficiency bounds for testing a multiparticle bell inequality in an asymmetric configuration, *Physical Review A* **108**, 052216 (2023).
- [10] B. Wittmann, S. Ramelow, F. Steinlechner, N. K. Langford, N. Brunner, H. M. Wiseman, R. Ursin, and A. Zeilinger, Loophole-free einstein-podolsky-rosen experiment via quantum steering, *New Journal of Physics* **14**, 053030 (2012).
- [11] P. H. Eberhard, Background level and counter efficiencies required for a loophole-free einstein-podolsky-rosen experiment, *Physical Review A* **47**, R747 (1993).
- [12] J. F. Clauser and M. A. Horne, Experimental consequences of objective local theories, *Physical Review D* **10**, 526 (1974).
- [13] S. Ramelow, A. Mech, M. Giustina, S. Gröblacher, W. Wieczorek, J. Beyer, A. Lita, B. Calkins, T. Gerrits, S. W. Nam, A. Zeilinger, and R. Ursin, Highly efficient heralding of entangled single photons, *Optics Express* **21**, 6707 (2013).
- [14] L. A. Ngah, O. Alibart, L. Labonté, V. D’Auria, and S. Tanzilli, Ultra-fast heralded single photon source based on telecom technology, *Laser & Photonics Reviews* **9**, doi.org/10.1002/lpor.201400404 (2015).
- [15] S. I. Davis, A. Mueller, R. Valivarthi, N. Lauk, L. Narvaez, B. Korzh, A. D. Beyer, O. Cerri, M. Colangelo, K. K. Berggren, M. D. Shaw, S. Xie, N. Sinclair, and M. Spiropulu, Improved heralded single-photon source with a photon-number-resolving superconducting nanowire detector, *Physical Review Applied* **18**, 064007 (2022).
- [16] L. Stasi, P. Caspar, T. Brydges, H. Zbinden, F. Bussières, and R. Thew, High-efficiency photon-number-resolving detector for improving heralded single-photon sources, *Quantum Science and Technology* **8**, 045006 (2023).
- [17] C. H. Bennett and G. Brassard, Quantum cryptography: Public key distribution and coin tossing, in *In Proceedings of IEEE International Conference on Computers* (1984).
- [18] M. Lucamarini, Z. L. Yuan, J. F. Dynes, and A. J. Shields, Overcoming the rate–distance limit of quantum key distribution without quantum repeaters, *Nature* **557**, 400–403 (2018).
- [19] S. Wang, D. Y. He, Z. Q. Yin, F. Y. Lu, C. H. Cui, W. Chen, Z. Zhou, G. C. Guo, and Z. F. Han, Beating the fundamental rate-distance limit in a proof-of-principle quantum key distribution system, *Physical Review X* **9**, 021046 (2019).
- [20] P. Zeng, H. Y. Zhou, W. J. Wu, and X. F. Ma, Mode-pairing quantum key distribution, *Nature Communications* **13**, 3903 (2022).
- [21] H. Kanamori, H. Yokota, G. Tanaka, M. Watanabe, Y. Ishiguro, I. Yoshida, T. Kakii, S. Itoh, Y. Asano, and S. Tanaka, Transmission characteristics and reliability of pure-silica-core single-mode fibers, *Journal of Lightwave Technology* **4**, 1144 (1986).
- [22] K. Nagayama, M. Kakui, M. Matsui, T. Saitoh, and Y. Chigusa, Ultra-low-loss (0.1484 db/km) pure silica core fibre and extension of transmission distance, *Electronics Letters* **38**, 1168 (2002).
- [23] M. Hirano, T. Haruna, Y. Tamura, T. Kawano, S. Ohnuki, Y. Yamamoto, Y. Koyano, and T. Sasaki, Record low loss, record high fom optical fiber with manufacturable process, in *Optical Fiber Communication Conference/National Fiber Optic Engineers Conference 2013*, PDP5A.7 (2013).
- [24] Y. Tamura, H. Sakuma, K. Morita, M. Suzuki, Y. Yamamoto, K. Shimada, Y. Honma, K. Sohma, T. Fujii, and T. Hasegawa, Lowest-ever 0.1419-dB/km loss optical fiber, in *2017 Optical Fiber Communications Conference and Exhibition (OFC)* (2017) pp. 1–3.
- [25] D. Gottesman, H. K. Lo, N. Lütkenhaus, and J. Preskill, Security of quantum key distribution with imperfect devices, *Quantum Information and Computation* **4**, 325 (2004).
- [26] H. Shu, Solve single photon detector problems, *Quantum* **7**, 1187 (2023).
- [27] H. Shu, Empty-signal detection: Proof-of-principle scheme for arbitrarily long-distance quantum communication (2025), arXiv:2509.15884 [quant-ph].
- [28] M. A. Albota and F. N. C. Wong, Efficient single-photon counting at 1.55 μm by means of frequency upconversion, *Optics Letters* **29**, 1449 (2004).
- [29] W. H. Jiang, J. H. Liu, Y. Liu, G. Jin, J. Zhang, and J. W. Pan, 1.25ghz sine wave gating ingaas/inp single-photon detector with a monolithically integrated readout circuit, *Optics Letters* **42**, 5090 (2017).
- [30] P. Hu, H. Li, L. X. You, H. Q. Wang, Y. Xiao, J. Huang, X. Y. Yang, W. J. Zhang, Z. Wang, and X. M. Xie, De-

- tecting single infrared photons toward optimal system detection efficiency, *Optics Express* **28**, 36884 (2020).
- [31] J. Chang, J. W. N. Los, J. O. Tenorio-Pearl, N. Noordzij, R. Gourgues, A. Guardiani, J. R. Zichi, S. F. Pereira, H. P. Urbach, V. Zwiller, S. N. Dorenbos, and I. Esmail Zadeh, Detecting telecom single photons with 99.5-2.07+0.5% system detection efficiency and high time resolution, *APL Photonics* **6**, 036114 (2021).
- [32] G. Z. Xu, W. J. Zhang, L. X. You, J. M. Xiong, X. Q. Sun, H. Huang, X. Ou, Y. M. Pan, C. L. Lv, H. Li, Z. Wang, and X. M. Xie, Superconducting microstrip single-photon detector with system detection efficiency over 90% at 1550nm, *Photonics Research* **9**, 958 (2021).
- [33] I. Craiciu, B. Korzh, A. D. Beyer, A. Mueller, J. P. Allmaras, L. Narváez, M. Spiropulu, B. Bumble, T. Lehner, E. E. Wollman, and M. D. Shaw, High-speed detection of 1550nm single photons with superconducting nanowire detectors, *Optica* **10**, 183 (2023).
- [34] J. P. Chen, C. Zhang, Y. Liu, C. Jiang, W. J. Zhang, X. L. Hu, J. Y. Guan, Z. W. Yu, H. Xu, J. Lin, M. J. Li, H. Chen, H. Li, L. X. You, Z. Wang, X. B. Wang, Q. Zhang, and J. W. Pan, Sending-or-not-sending with independent lasers: Secure twin-field quantum key distribution over 509 km, *Physical Review Letters* **124**, 070501 (2020).
- [35] L. Zhou, J. P. Lin, Y. M. Xie, Y. S. Lu, Y. M. Jing, H. L. Yin, and Z. L. Yuan, Experimental quantum communication overcomes the rate-loss limit without global phase tracking, *Physical Review Letters* **130**, 250801 (2023).
- [36] Y. Liu, W. J. Zhang, C. Jiang, J. P. Chen, C. Zhang, W. X. Pan, D. Ma, H. Dong, J. M. Xiong, C. J. Zhang, H. Li, R. C. Wang, J. Wu, T. Y. Chen, L. X. You, X. B. Wang, Q. Zhang, and J. W. Pan, Experimental twin-field quantum key distribution over 1000 km fiber distance, *Physical Review Letters* **130**, 210801 (2023).
- [37] I. Charaev, E. K. Batson, S. Cherednichenko, K. Reidy, V. Drakinskiy, Y. Yu, S. Lara-Avila, J. D. Thomsen, M. Colangelo, F. Incalza, K. Ilin, A. Schilling, and K. K. Berggren, Single-photon detection using large-scale high-temperature mgb2 sensors at 20 k, *Nature Communications* **15**, 3973 (2024).
- [38] PsiQuantum, A manufacturable platform for photonic quantum computing, *Nature* **641**, doi.org/10.1038/s41586-025-08820-7 (2025).
- [39] S. Krastanov, M. Heuck, J. H. Shapiro, P. Narang, D. R. Englund, and K. Jacobs, Room-temperature photonic logical qubits via second-order nonlinearities, *Nature Communications* **12**, doi.org/10.1038/s41467-020-20417-4 (2021).
- [40] M. Heuck, D. R. Englund, and K. Jacobs, Efficient, high-speed two-photon logic gates at room temperature for general-purpose quantum information processing (2023), filed Mar. 3, 2020, Application No. 16/807,662.
- [41] K. Sengupta, S. P. Dinesh, K. M. Shafi, S. Asokan, and C. M. Chandrashekar, Experimental realization of universal quantum gates and a six-qubit entangled state using a photonic quantum walk, *Physical Review Applied* **24**, 024012 (2025).
- [42] S. Austin, D. Devulapalli, K. Hoang, F. Zhou, K. Srinivasan, and A. V. Gorshkov, A vapor-cavity-qed system for quantum computation and communication (2025), arXiv:2509.19432 [quant-ph].
- [43] T. P. Harty, D. T. C. Allcock, C. J. Ballance, L. Guidoni, H. A. Janacek, N. M. Linke, D. N. Stacey, and D. M. Lucas, High-fidelity preparation, gates, memory, and read-out of a trapped-ion quantum bit, *Physical Review Letters* **113**, 10.1103/physrevlett.113.220501 (2014).
- [44] M. Melchiorri, N. Daldosso, F. Sbrana, L. Pavesi, G. Pucker, C. Kompocholis, P. Bellutti, and A. Lui, Propagation losses of silicon nitride waveguides in the near-infrared range, *Applied Physics Letters* **86** (2005).
- [45] A. Chanana, H. Larocque, R. Moreira, J. Carolan, B. Guha, E. G. Melo, V. Anant, J. D. Song, D. Englund, D. J. Blumenthal, K. Srinivasan, and M. Davanco, Ultra-low loss quantum photonic circuits integrated with single quantum emitters, *Nature Communications* **13**, 7693 (2022).
- [46] L. T. Feng, M. Zhang, X. Xiong, D. Liu, Y. J. Cheng, F. M. Jing, X. Z. Qi, Y. Chen, D. Y. He, G. P. Guo, G. C. Guo, D. X. Dai, and X. F. Ren, Transverse mode-encoded quantum gate on a silicon photonic chip, *Physical Review Letters* **128**, 10.1103/physrevlett.128.060501 (2022).
- [47] L. T. Feng, M. Zhang, D. Liu, Y. J. Cheng, X. Y. Song, Y. Y. Ding, D. X. Dai, G. P. Guo, G. C. Guo, and X. F. Ren, Chip-to-chip quantum photonic controlled-not gate teleportation, *Physical Review Letters* **135**, 020802 (2025).
- [48] A. Laing, A. Peruzzo, A. Politi, M. R. Verde, M. Halder, T. C. Ralph, M. G. Thompson, and J. L. O'Brien, High-fidelity operation of quantum photonic circuits, *Applied Physics Letters* **97**, 211109 (2010).
- [49] A. Crespi, R. Ramponi, R. Osellame, L. Sansoni, I. Bongioanni, F. Sciarrino, G. Vallone, and P. Mataloni, Integrated photonic quantum gates for polarization qubits, *Nature Communications* **2**, doi.org/10.1038/ncomms1570 (2011).
- [50] J. Piasetzky, A. Rotem, Y. Warshavsky, Y. Drori, K. Cohen, Y. Oz, and H. Suchowski, High fidelity cnot gates in photonic integrated circuits using composite segmented directional couplers (2025), arXiv:2509.25505 [physics.optics].
- [51] H. Nakav, T. Firdoshi, O. Davidson, B. C. Das, and O. Firstenberg, Quantum cnot gate with actively synchronized photon pairs (2025), arXiv:2505.03960 [quant-ph].
- [52] S. A. H. Gangaraj and D. T. Nguyen, Quantum photonic gates with two-dimensional random walkers, *Optics Express* **33**, 11264 (2025).
- [53] K. B. Dideriksen, R. Schmiege, M. Zugenmaier, and E. S. Polzik, Room-temperature single-photon source with near-millisecond built-in memory, *Nature Communications* **12**, 10.1038/s41467-021-24033-8 (2021).
- [54] J. Wang, S. Paesani, Y. Ding, R. Santagati, P. Skrzypczyk, A. Salavrakos, J. Tura, R. Augusiak, L. Mančinska, D. Bacco, D. Bonneau, J. Silverstone, Q. Gong, A. Acín, K. Rottwitt, L. Oxenlowe, J. O'Brien, A. Laing, and M. Thompson, Large-scale integration of multidimensional quantum photonics circuits on silicon, in *2018 Conference on Lasers and Electro-Optics (CLEO)* (2018) pp. 1–2.
- [55] J. W. Wang, S. Paesani, Y. H. Ding, R. Santagati, P. Skrzypczyk, A. Salavrakos, J. Tura, R. Augusiak, L. Mančinska, D. Bacco, D. Bonneau, J. W. Silverstone, Q. H. Gong, A. Acín, K. Rottwitt, L. K. Oxenlowe, J. L. O'Brien, A. Laing, and M. G. Thompson, Multidimensional quantum entanglement with large-scale integrated optics, *Science* **360**, 285 (2018).

- [56] S. Paesani, Y. H. Ding, R. Santagati, L. Chakhmakhchyan, C. Vigliar, K. Rottwitt, L. K. Oxenløwe, J. W. Wang, M. G. Thompson, and A. Laing, Generation and sampling of quantum states of light in a silicon chip, *Nature Physics* **15**, 925–929 (2019).
- [57] S. Yu, W. Liu, S. J. Tao, Z. P. Li, Y. T. Wang, Z. P. Zhong, R. Patel, Y. Meng, Y. Z. Yang, Z. A. Wang, N. J. Guo, X. D. Z., Z. Chen, L. Xu, N. Zhang, X. Liu, M. Yang, W. H. Zhang, Z. Q. Zhou, and G. C. Guo, A von-neumann-like photonic processor and its application in studying quantum signature of chaos, *Light, science & applications* **13**, 74 (2024).
- [58] J. M. Bao, Z. R. Fu, T. Pramanik, J. Mao, Y. L. Chi, Y. K. Cao, C. H. Zhai, Y. F. Mao, T. X. Dai, X. J. Chen, X. Y. Jia, L. S. Zhao, Y. Zheng, B. Tang, Z. H. Li, J. Luo, W. W. Wang, Y. Yang, Y. Y. Peng, and J. W. Wang, Very-large-scale integrated quantum graph photonics, *Nature Photonics* **17**, 1 (2023).
- [59] C. Taballione, T. A. W. Wolterink, J. Lugani, A. Eckstein, B. A. Bell, R. Grootjans, I. Visscher, D. Geskus, C. G. H. Roeloffzen, J. J. Renema, I. A. Walmsley, P. W. H. Pinkse, and K. J. Boller, 8×8 reconfigurable quantum photonic processor based on silicon nitride waveguides, *Optics Express* **27**, 26842 (2019).
- [60] B. Desiatov, A. Shams-Ansari, M. Zhang, C. Wang, and M. Lončar, Ultra-low-loss integrated visible photonics using thin-film lithium niobate, *Optica* **6**, 380 (2019).